ECS Transactions, 3 (25) 249-258 (2007)
10.1149/1.2753257, copyright The Electrochemical Society

# Design and Fabrication of High Anisotropy Nanoscale Bit-Patterned Magnetic Recording Medium for Data Storage Applications (invited)

D. Litvinov[a,b], Ch. E[a], V. Parekh[a], D. Smith[c], J. Rantschler[a], S. Zhang[b], W. Donner[d], T.R. Lee[e], P. Ruchhoeft[a], Dieter Weller[f], and S. Khizroev[g]

[a] Electrical & Computer Engineering, University of Houston, Houston, TX
[b] Chemical & Biomolecular Engineering, University of Houston, Houston, TX
[c] Materials Engineering, University of Houston, Houston, TX
[d] Physics, University of Houston, Houston, TX
[e] Chemistry, University of Houston, Houston, TX
[f] Seagate Technology, Fremont, CA
[g] Electrical Engineering, University of California, Riverside, CA

Design considerations for bit-patterned magnetic medium for next generation data storage systems is presented. $(Co/Pd)_N$ magnetic multilayers are evaluated as candidates for bit-patterned medium recording layer materials for their high and easily tunable magnetic anisotropy. Optimized patterned multilayers used in this study had coercivities in excess of 12-14kOe. Bit patterning was accomplished using ion-beam proximity printing, a high-throughput direct write lithography where a large array of ion beamlets shaped by a stencil mask is used to write an arbitrary device pattern. It is found that the nature of magnetization reversal strongly depends on bit edge imperfections and is likely to contribute to switching field distribution.

## Introduction

Conventional magnetic recording systems based on longitudinal magnetic recording are rapidly approaching their superparamagnetic limit(1,2). A shift to perpendicular recording(3) is taking place due to its superiority with respect to data thermal stability.(3,4) Yet, perpendicular recording will face its own superparamagnetic limit(5), which calls for further innovation. Magnetic recording based on patterned media(6,7), as compared to continuous media used in today's hard drives, allows to further extend areal bit densities due to a significant increase of the thermal activation volume(8). In patterned media, the data are stored in an array of discrete elements, nanomagnets, as illustrated in Figure 1.

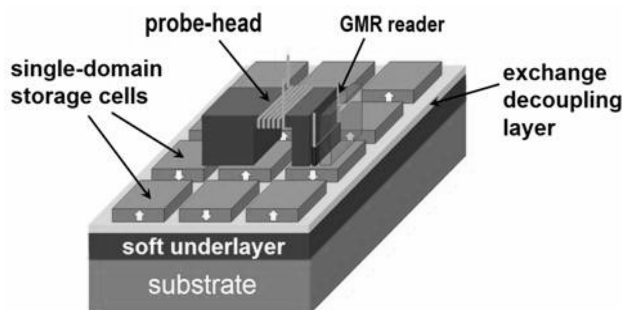


Figure 1: A schematic of a patterned medium recording system.

Downloaded on 2016-02-20 to IP 130.203.136.75 address. Redistribution subject to ECS terms of use (see ecsdl.org/site/terms_use) unless CC License in place (see abstract).

In this work, we present medium materials design considerations, discuss application of exchange-coupled high-anisotropy magnetic multilayers for bit-patterned recording layers, evaluate factors affecting magnetization reversal, discuss medium patterning using ion beam proximity lithography (9,10), and evaluate magnetic properties of bit-patterned medium prototypes.

## Materials for Bit-Patterned Media Recording Layers

### Materials Design Considerations

The bits in a patterned medium recording layer are pre-defined by the medium manufacturing process. This leads to one of the key issues in patterned medium recording design – write synchronization, the loss of which causes the write pulse to be applied in the interior of a bit. If a conventional "exchange de-coupled" medium is utilized, individual grains can be switched independently and the loss of synchronization will lead to writing "bit transitions" inside the bits as illustrated in Figure 2.

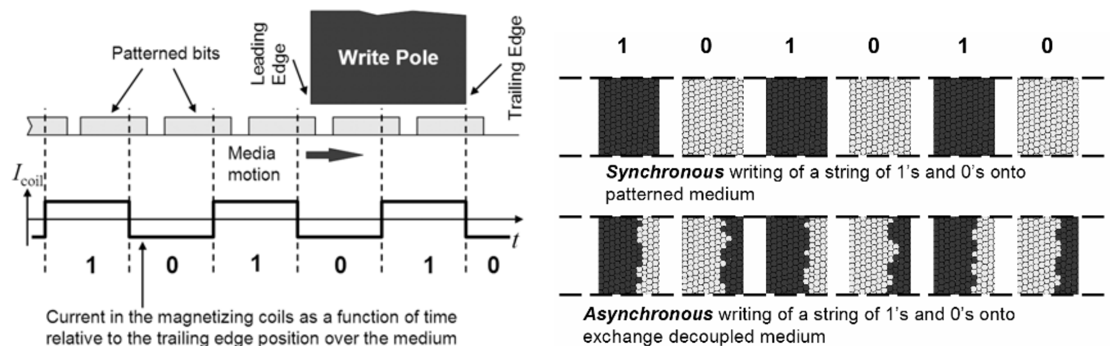


Figure 2. Schematics of synchronous and asynchronous writing on patterned medium with exchange decoupled magnetic grains.

Enhanced intergranular exchange coupling in the recording layer material addresses this issue forcing the patterned bit to act as a *single magnetic domain* when the bit size is comparable to or smaller than the characteristic exchange length, $\delta$, given by $\delta = \pi\sqrt{A / K_{Ueff}}$ , where $K_{Ueff}$ is the effective anisotropy energy that takes into account demagnetizing fields and $A$ is exchange stiffness. The magnetization of such single domain bits cannot be partially switched, resulting in synchronous-like writing even when synchronization is partially lost. It should be noted that severe synchronization errors will lead to inability to write at all and should be avoided.

Among the candidates for a patterned medium recording layer are conventional CoCrX alloys where X refers to various additives such as Pt, Ta, Nb, B, magnetic multilayers such as $(Co/Pd)_N$, where N defines the number of bi-layers, and $L1_0$ alloys such as FePt. CoCrX alloys are employed in conventional continuous medium recording and are of interest due to the wealth of available information on the synthesis and properties of this class of materials (11,12). However, the limitations on the maximum achievable magnetic anisotropy leave open questions whether this class of materials is appropriate for patterned magnetic medium and whether CoCrX alloys would allow technology extensibility(13). Additionally, the development of vertical texture to achieve



Downloaded on 2016-02-20 to IP 130.203.136.75 address. Redistribution subject to ECS terms of use (see ecsdl.org/site/terms_use) unless CC License in place (see abstract).

perpendicular magnetic anisotropy usually requires an energetic process involving deposition at high temperature and/or substrate bias. Such deposition conditions usually result in Cr segregation at grain boundaries and exchange decoupling of magnetic grains, which is undesirable in case of patterned medium. $L1_0$ alloys are characterized by very large magnetic anisotropies compatible with future generations of ultra-high density data storage (14). However, questions remain related to the processing issues involved in fcc→fct transformation that are yet to be addressed (15,16).

Magnetic Multilayers

Magnetic multilayers such as $(Co/Pd)_n$ exhibit very large and easily tunable vertical magnetic anisotropies (17,18) which makes them suitable for ultra-high density magnetic recording applications(19). The anisotropy in these materials results from *d*-shell electron hybridization at the interfaces between the cobalt and palladium layers. The magnitude of the anisotropy can be tuned by controlling the quality of the interfaces and/or by changing the thicknesses of individual layers. As applied to patterned medium recording, high intergranular exchange coupling is required to suppress the possibility of writing bit transitions inside the bits due to write synchronization errors(20). The films need to be highly uniform (magnetically) to minimize switching field distribution of individual patterned bits. By comparison, magnetic defects as a means to pin magnetic domain walls are commonly introduced into magnetic multilayers to enable large coercivities (21,22).

In this work, magnetic films were deposited by magnetron sputtering at room temperature on thermal oxide coated Si wafers. A 5nm Ta seed layer was used to promote exchange coupled films (22). Soft underlayers (23) were not used in this work to simplify magnetic characterization. TEM micrographs of $(Co/Pd)_N$ multilayers deposited on Ta and indium-tin-oxide (ITO) (optimized for continuous medium recording) buffer layers are shown in Figure 3a-b (16,24). Low density regions designed for exchange decoupling can be noticed in the film optimized for continuous medium.

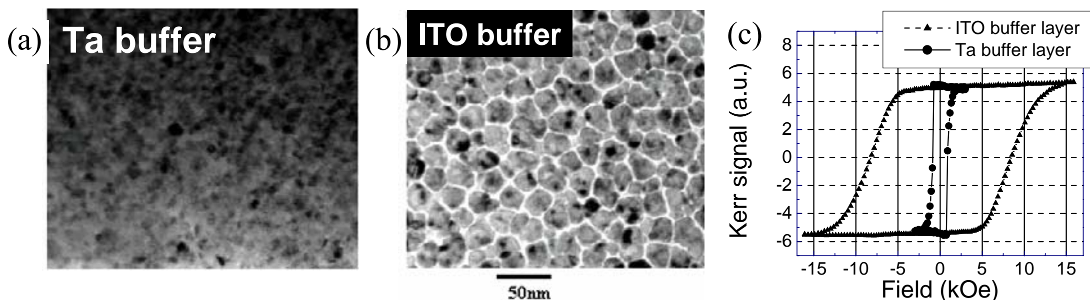


Figure 3. In-plane TEM micrographs of $(Co/Pd)_n$ multilayers grown on (a) Ta and (b) ITO buffer layers. (c) Vertical M-H loops for $(Co/Pd)_n$ multilayer films grown on Ta and ITO buffers. Ta buffer leads to highly exchange coupled films. ITO buffer results in "granular" medium infused with low density exchange de-coupling regions.

Vertical M-H loops for typical exchange-coupled and exchange-decoupled columnar multilayer films are compared in Figure 3c. It should be emphasized that large coercivity cannot and should not be used as a figure of merit for exchange-coupled multilayer films designed for patterned medium applications since the coercivity in these materials is controlled mostly by the domain wall pinning strength, which is ideally

Downloaded on 2016-02-20 to IP 130.203.136.75 address. Redistribution subject to ECS terms of use (see ecsdl.org/site/terms_use) unless CC License in place (see abstract).

minimized (18). The deposition conditions and the thicknesses of individual Co (3Å) and Pd (7Å) layers were optimized to achieve largest vertical anisotropy, smallest coercivity (to minimize domain wall pinning), and remnant squareness of one. It should be noted that optimized films had a surface roughness of ≤1nm as measured using atomic force microscopy.

### Magnetization Reversal in Bit-Patterned Media

Magnetization reversal in patterned bits under application of external magnetic field is illustrated in Figure 4 where two distinct cases of magnetization evolution in a 50nm bit as a function time calculated using LLG Micromagnetic Simulator (25) are shown. Parameters used in these simulations included an anisotropy field, Hk, of 25kOe, a saturation magnetization, $M_S$, of 400 emu/cc, and an exchange stiffness, A, of 1.05μerg/cm. Bit thickness was kept at 10nm. In general, magnetization reversal takes place by domain wall injection and propagation on a time scale of 1-2 ns. The specifics of the reversal strongly depend on the bit geometry. In case of "perfect" bits with vertical sidewalls, a bubble domain nucleates at the center of a bit and expands radially reversing the magnetization of the bit as shown in Figure 4a. In a more realistic case of bits with tapered sidewalls, domain walls nucleate at bit edges and sweep across the bits reversing the magnetization orientation as illustrated in Figure 4b. The two processes are not energetically equivalent and are expected to contribute to increased switching field distribution (SFD) in realistic bit-patterned media. Moreover, continuous bit edge variations such as line edge roughness and tapering angle variations are also expected to contribute wider SFD.

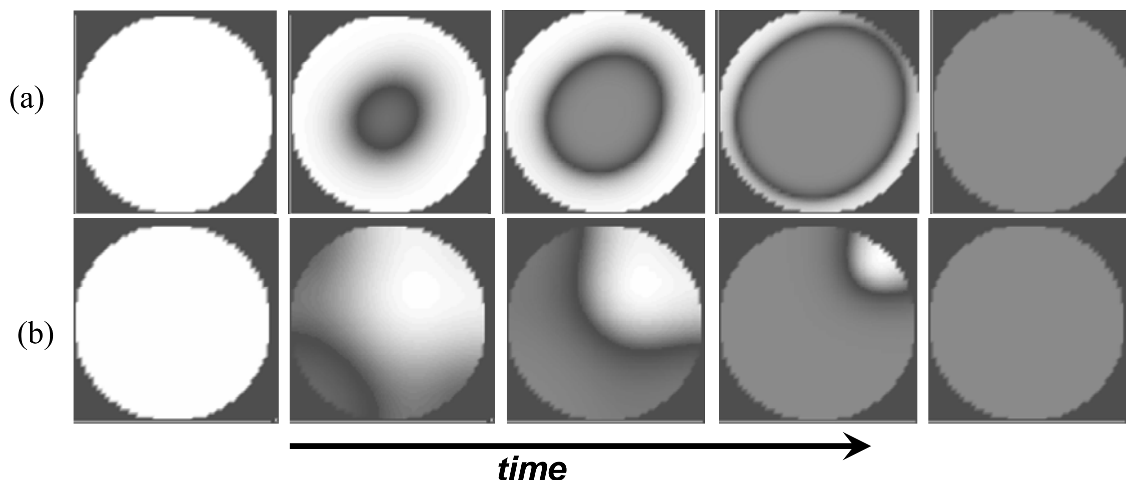


Figure 4: Magnetization evolution during magnetization reversal in a 50nm bit with (a) straight sidewalls and (b) sidewalls tapered at 45°.

The dependences of the magnitude of the reversal field on the bit size and bit sidewall tapering angle are shown in Figure 5. The dependence of the reversal field on the bit size is stronger for smaller bits. For 50nm bits, a bit size variation of 5% contributes approximately 5% to the SFD. Variations in the bit sidewall angle between 90 degrees (perfect bit) and 45 degrees result in additional 5% contribution to SFD.


Downloaded on 2016-02-20 to IP 130.203.136.75 address. Redistribution subject to ECS terms of use (see ecsdl.org/site/terms_use) unless CC License in place (see abstract).

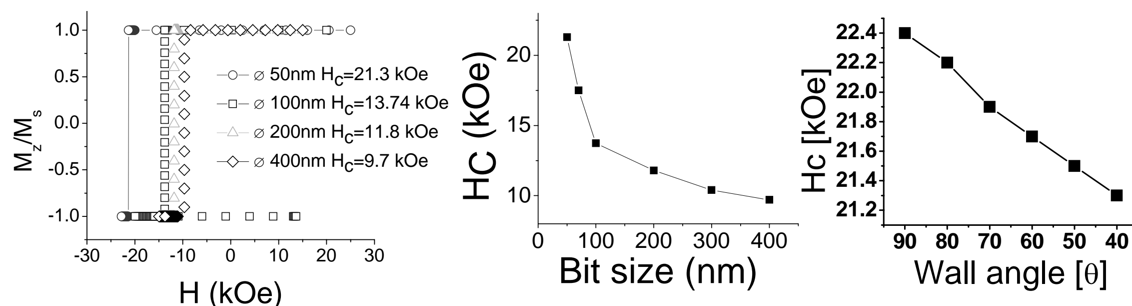


Figure 5. (left) Simulated M-H loops for different diameter patterned bits; (center) dependence of coercivity on bit size; (right) dependence of the coercivity on the bit sidewall tapering.

## Medium Patterning

Ion-Beam Proximity Lithography

Medium patterning was accomplished using ion-beam proximity lithography (IBPL) (9,26), a high-throughput direct write lithography where a large array of ion beamlets shaped by a stencil mask is used to write an arbitrary periodic device pattern as illustrated in Figure 6. In IBPL system used in this work, helium ions are extracted from a duo-plasmatron ion source, accelerated through a constant gradient tube, and drift towards a mask placed about 10m downstream. A 30 keV $He^+$ ion-beam with an ion current density of 140nA/cm$^2$ was used. Integration of the beam current measured using a Faraday cup provides the exposure dose. Parallel-plates electrostatic x-y deflectors placed at 50cm away from the silicon nitride stencil membrane(27) and driven by four high-voltage operational amplifiers enable the deflection of the ion beamlets to obtaining an arbitrary high density pattern.

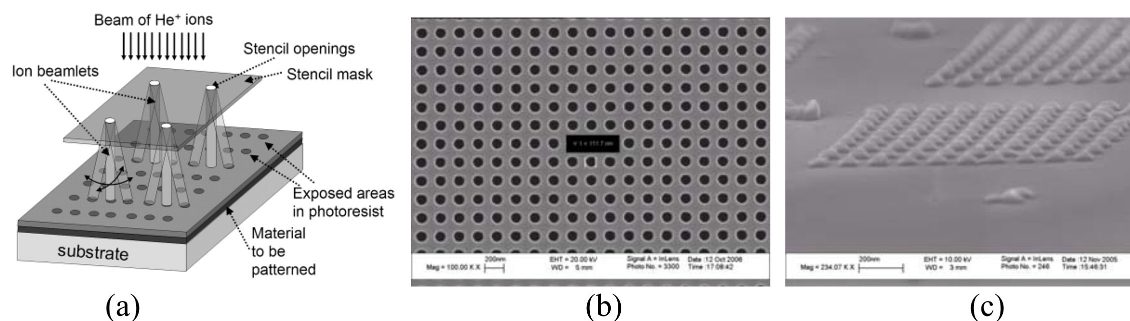


Figure 6: (a) A schematic of the ion-beam proximity lithography system. Electrostatic field deflection is used to replicate a sparse stencil mask into high density pattern; (b) a SEM image of silicon nitride stencil mask with 110nm stencil openings; (c) a 10x10 bit-patterned medium array printed using IBPL.

Pattern Transfer

A preferred approach to pattern transfer is utilizing a negative resist to directly define patterned transfer etch masks. In this approach, hydrogen silsesquioxane (HSQ), a high resolution negative tone resist (28) is spun onto magnetic multilayer coated wafers

Downloaded on 2016-02-20 to IP 130.203.136.75 address. Redistribution subject to ECS terms of use (see ecsdl.org/site/terms_use) unless CC License in place (see abstract).

and exposed in a IBPL systems (typical dose of 9μC/cm$^2$ is used). The deflection plates are used to print multiple, offset images and, in such, adjust the desired pattern density. Using HSQ as a hard mask, the samples are then sputter-etched or ion-milled to transfer the resist pattern into the multilayer film(29). It should be noted that sputter-etching does not lead to measurable changes of the magnetic properties of the film protected by HSQ. Reactive ion etching (RIE) using $CHF_3$ is used to remove HSQ. An SEM micrograph of a patterned medium prototype with 43nm features on a 135nm pitch is shown in Figure 7. Alternatively, positive resist such a polymethyl metacrylate (PMMA) can be used. However, a tone reversal step using metal (e.g. aluminum) evaporation and lift-off is required in this approach and imposes limitations on the achievable packing density.

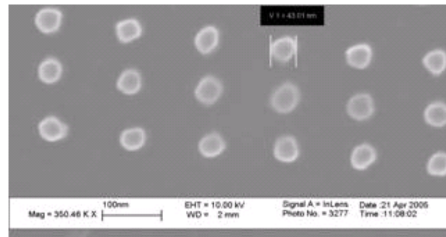

Figure 7: An SEM micrograph of a patterned medium sample with 43nm magnetic islands on a 135nm pitch.

It should be noted that in contrast to the related work by Chappert et.al.(30) where magnetic patterning was achieved via selective area ion-mixing of the multilayer thin films (31), in IBPL, magnetic material is physically removed to form exchange decoupled magnetic islands. Moreover, the effect of ion-mixing at the edges of nominally unexposed regions is limited to 1-2nm (as confirmed by Monte-Carlo simulations(32)) and can be addressed if necessary via a short post-patterning overetch.

## Patterned Medium Characterization

### Magnetic Properties of Patterned vs. Continuous Magnetic Multilayers

Vertical M-H loops for a continuous and patterned multilayer samples are compared in Figure 8a. A significant increase in the coercivity of patterned samples observed in Figure 8a results from domain wall pinning by physical barriers (non-magnetic trenches) formed between adjacent bits (29). A combinatorial approach was used to evaluate coercivity dependence on Co and Pd layer thicknesses for continuous and patterned multilayers shown in Figure 8b and Figure 8c, respectively. In the utilized approach, a combinatorial magnetic multilayer library is deposited onto a wafer, where the thicknesses of individual layers in the Co/Pd bi-layer stack are varied across the wafer, in a single deposition run to ensure identical deposition conditions (33). Different regions of the combinatorial wafer are then patterned and their properties are evaluated. Significantly, combinatorial approach ensures identical synthesis conditions and, consequently, enables accurate comparisons. As seen in Figure 8b-c, coercivities of continuous and patterned films exhibit similar trends with respect to Co and Pd layer thickness variations. Thus, the coercivity trend in continuous multilayer films deposited at identical deposition conditions can be used as an indicator of expected coercivity trend in patterned multilayer films.



Downloaded on 2016-02-20 to IP 130.203.136.75 address. Redistribution subject to ECS terms of use (see ecsdl.org/site/terms_use) unless CC License in place (see abstract).

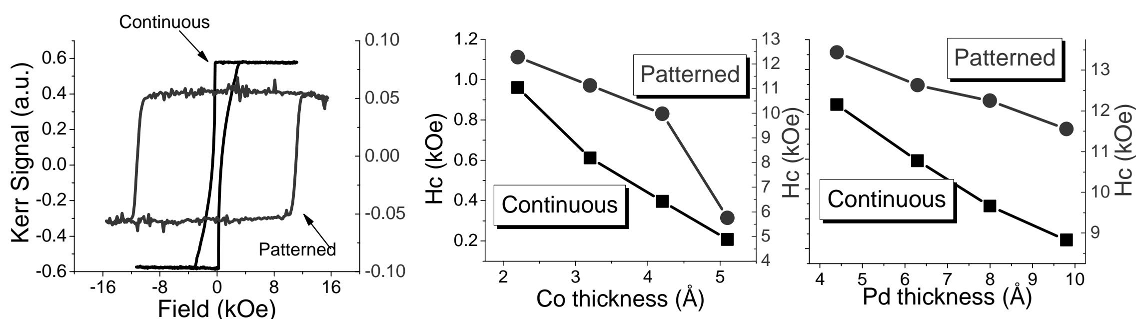


Figure 8. (a) Easy axis M-H loops for continuous and patterned Co(3.2Å)/Pd(6.3 Å) multilayer films; (b) cobalt and (c) palladium thickness dependence of easy axis coercivity. 200nm islands on a 500nm pitch were used.

However, as seen in Figure 9, the above observation is not valid if applied to films prepared at different deposition conditions, e.g., at different sputtering pressures. Although higher deposition pressures result in higher coercivity of continuous multilayers, the coercivity of patterned films, a parameter reflecting magnetic anisotropy, is significantly enhanced in films prepared at lower deposition pressure. Significantly, the values of saturation magnetization, $M_S$, for the multilayers (and demagnetizing fields) deposited at different pressures remain unchanged and cannot account for the variation in the coercivity. The origin of high magnetic anisotropy is improved crystallinity (better film texture and larger grain size) as seen from Figure 9.

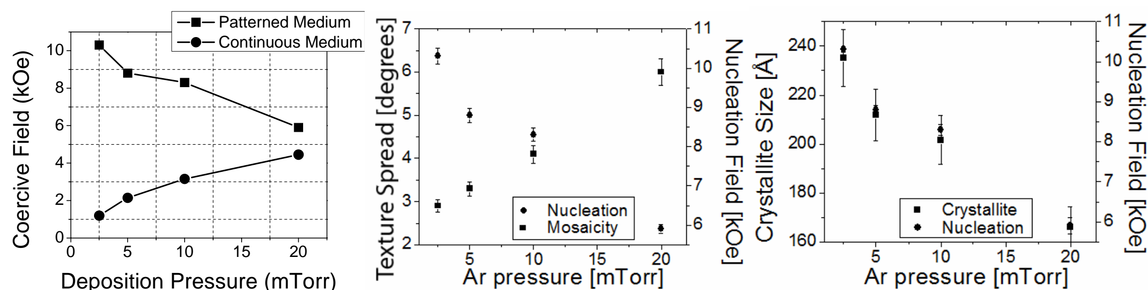


Figure 9. (left) Coercivity as a function of deposition pressure for continuous and patterned $[Co(3Å)/Pd(7Å)]_{30}$ multilayer films; (center) Comparison of nucleation field values and film mosaicity (texture spread) for multilayers sputtered at different pressures; (right) Comparison of nucleation field values and crystallite size for multilayers sputtered at different pressures.

## Magnetics Anisotropy and Hybridization of d-Shell Electrons at Co/Pd Interfaces

For completeness, the valence position of the multilayers as a function of Co thickness for several deposition pressures is shown in Figure 10a. The decrease of the binding energy with the increasing Co thickness correlated with the observed decrease in magnetic anisotropy with the increasing Co thickness. Moreover, the binding energies for 20 mT samples are significantly closer to the valence position of pure Co than pure Pd, which is in agreement with the decrease in anisotropy field of the samples with increasing deposition pressure observed in Figure 9. Weaker hybridization of Pd atoms for samples with thicker Co layers and deposited at higher pressures results in lower anisotropy.


Downloaded on 2016-02-20 to IP 130.203.136.75 address. Redistribution subject to ECS terms of use (see ecsdl.org/site/terms_use) unless CC License in place (see abstract).

Significantly, no measurable d-electron hybridization was observed for as deposited CoPd alloys.

Pd atoms located further from the interface should experience less hybridization, and hence less magnetic moment than the Pd atoms located immediately at the interface. XPS measurements yield an average for all of the layers within the probing depth of the material, so if the additional Pd monolayers are not hybridized as strongly as those at the interface we expect to see a drop in the valence position energy (closer to the position of pure Pd). Indeed, as the thickness of the Pd layer in the multilayer structure increases, the valence position shifts toward the Pd baseline sample as shown in Figure 10b. This is in agreement with ab initio calculations (34) have shown that the Pd atoms nearest to the interface acquire a magnetic moment of $0.30\mu_B$ due to d-electron hybridization, whereas the second layer from the interface only $0.17\mu_B$ and the third layer $0.03\mu_B$.

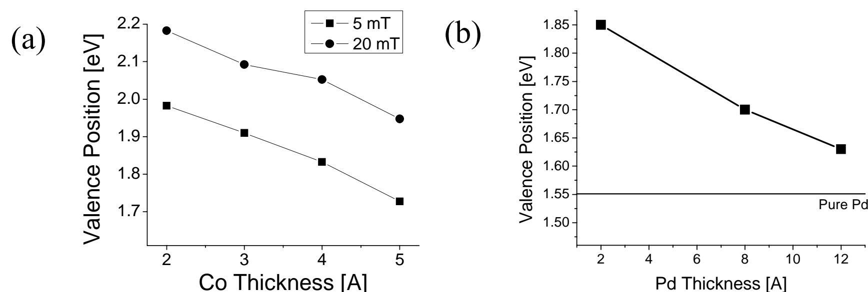


Figure 10. (a) Valence position of the $[Co(X)/Pd(7Å)]_{30}$ films sputtered at 5mT and 20mT deposition pressures; (b) Valence position of the $[Co(3Å)/Pd(X)]_{30}$ films sputtered at 2.5 mTorr.

<u>Switching Field Distribution</u>

As can be seen from Figure 11, SFD can be directly extracted from the hysteresis loops, which nearly exactly overlap with the remnance curves. This, in general, simplifies the characterization of the switching field distribution. Relatively large SFD of about 10% or 1kOe is likely the result of bit size variations (~4% in this case) and bit edge non-uniformities discussed in the text above.

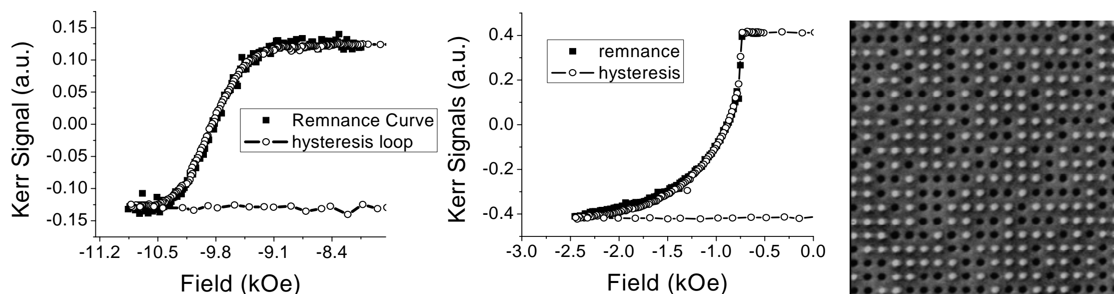


Figure 11. Vertical hysteresis loops and remnance curves for patterned (left) and continuous (center) multilayer films; (right) Typical MFM image of a remnant state in a bit-patterned medium with 200nm bits.


Downloaded on 2016-02-20 to IP 130.203.136.75 address. Redistribution subject to ECS terms of use (see ecsdl.org/site/terms_use) unless CC License in place (see abstract).

## Summary

Fabrication of patterned medium prototypes using ion-beam proximity lithography is demonstrated. High anisotropy exchange coupled $(Co/Pd)_N$ magnetic multilayers are evaluated as potential bit-patterned recording layer materials. Micromagnetic study of magnetization reversal indicates potentially significant influence of bit edge imperfections on switching field distribution. The deviation of vertical M-H loops from perfect squareness is attributed to finite switching field distribution. Direct correlation between d-electron hybridization and magnetic anisotropy is demonstrated.

## Acknowledgments

This work was conducted at the Center for Nanomagnetic Systems at the University of Houston. The authors would like to express their gratitude to Paul Frank of INSIC and Jack Wolfe of University of Houston for insightful discussions. This work was supported by the grants from National Science Foundation (ECS-0404308, ECS-0421255, ECS-0401297), Information Storage Industry Consortium, and AFOSR.

## References

1. H. N. Bertram and M. Williams, *IEEE Trans. Magn.* **36** (1), 4 (2000).
2. P. L. Lu and S. Charap, *IEEE Trans. Magn.* **30** (6), 4230 (1994).
3. S. Khizroev and D. Litvinov, *Perpendicular Magnetic Recording*. (Kluwer Academic Publishers, Dordrecht, The Netherlands, 2004).
4. D. Clark, in *Wall Street Journal* (New York, NY, 2005), pp. B.7.
5. M. Mallary, A. Torabi, and M. Benakli, *IEEE Trans. Magn.* **38** (4), 1719 (2002).
6. G. F. Hughes, *IEEE Trans. Magn.* **36** (2), 521 (2000).
7. E. D. Boerner, H. N. Bertram, and G. F. Hughes, *J. Appl. Phys.* **85** (8), 5318 (1999).
8. M. Albrecht, S. Anders, T. Thomson, C. T. Rettner, M. E. Best, A. Moser, and B. D. Terris, *J. Appl. Phys.* **91** (10), 6845 (2002).
9. P. Ruchhoeft and J. C. Wolfe, *J. Vac. Sci. Technol. B* **19** (6), 2529 (2001).
10. J. C. Wolfe, S. V. Pendharkar, P. Ruchhoeft, S. Sen, M. D. Morgan, W. E. Horne, R. C. Tiberio, and J. N. Randall, *J. Vac. Sci. Technol. B* **14** (6), 3896 (1996).
11. J.C. Lodder, D. D. Wind, G.E.v. Dorssen, T.J.A. Pompa, and A. Hubert, *IEEE Trans. Magn.* **23**, 214 (1987).
12. B. Lu, D. Weller, G. P. Ju, A. Sunder, D. Karns, M. L. Wu, and X. W. Wu, *IEEE Trans. Magn.* **39** (4), 1908 (2003).
13. D. Weller and A. Moser, *IEEE Trans. Magn.* **35** (6), 4423 (1999).
14. T. Klemmer, D. Hoydick, H. Okumura, B. Zhang, and W. A. Soffa, *Scripta Metallurgica Et Materialia* **33** (10-11), 1793 (1995).
15. B. Cheong and D. E. Laughlin, *Scripta Metallurgica Et Materialia* **29** (6), 829 (1993).
16. J. H. Judy, *J. Magn. Magn. Mater.* **287**, 16 (2005).
17. P. F. Carcia, *J. Appl. Phys.* **63** (10), 5066 (1988).
18. C. F. Brucker, *J. Appl. Phys.* **70** (10), 6065 (1991).
19. C. Brucker, T. Nolan, B. Lu, Y. Kubota, M. Plumer, P. L. Lu, R. Cronch, C. H. Chang, D. Chen et al., *IEEE Trans. Magn.* **39** (2), 673 (2003).



Downloaded on 2016-02-20 to IP 130.203.136.75 address. Redistribution subject to ECS terms of use (see ecsdl.org/site/terms_use) unless CC License in place (see abstract).

20. Chunsheng; E, D; Smith, J.; Wolfe, D; Weller, S.; Khizroev, and D. Litvinov, *J. Appl. Phys.* **98** (1) (2005).
21. C. H. Chang and M. H. Kryder, *J. Appl. Phys.* **75** (10), 6864 (1994).
22. D. Litvinov, T. Roscamp, T. J. Klemmer, M. Wu, J.K. Howard, and S. Khizroev, *Materials Research Society Symposium Proceedings* **674**, T3.9 (2001).
23. D. Litvinov, M. H. Kryder, and S. Khizroev, *J. Magn. Magn. Mater.* **232** (1-2), 84 (2001).
24. A. G. Roy, D. E. Laughlin, T. J. Klemmer, K. Howard, S. Khizroev, and D. Litvinov, *J. Appl. Phys.* **89** (11), 7531 (2001).
25. M.R. Scheinfein, LLG Micromagnetic Simulator (2005).
26. D. P. Stumbo, G. A. Damm, S. Sen, D. W. Engler, F. O. Fong, J. C. Wolfe, and J. A. Oro, *J. Vac. Sci. Technol. B* **9** (6), 3597 (1991).
27. K. P. Han, W. D. Xu, A. Ruiz, P. Ruchhoeft, and S. Chellam, *Journal Of Membrane Science* **249** (1-2), 193 (2005).
28. M. J. Word, I. Adesida, and P. R. Berger, *J. Vac. Sci. Technol. B* **21** (6), L12 (2003).
29. V. Parekh, E. Chunsheng, D. Smith, A. Ruiz, J. C. Wolfe, P. Ruchhoeft, E. Svedberg, S. Khizroev, and D. Litvinov, *Nanotechnology* **17** (9), 2079 (2006).
30. C. Chappert, H. Bernas, J. Ferre, V. Kottler, J. P. Jamet, Y. Chen, E. Cambril, T. Devolder, F. Rousseaux et al., *Science* **280** (5371), 1919 (1998).
31. T. Devolder, C. Chappert, and H. Bernas, *J. Magn. Magn. Mater.* **249** (3), 452 (2002).
32. J.F. Ziegler, SRIM/TRIM (2003).
33. Ch. E, D. Smith, E. Svedberg, S. Khizroev, and D. Litvinov, *J. Appl. Phys.* **99** (11) (2006).
34. M. Cinal and D. M. Edwards, *Phys. Rev. B* **55** (6), 3636 (1997).




Downloaded on 2016-02-20 to IP 130.203.136.75 address. Redistribution subject to ECS terms of use (see ecsdl.org/site/terms_use) unless CC License in place (see abstract).